IOPscience iopscience.iop.org

Home Search Collections Journals About Contact us My IOPscience

Intermixing and composition profiles of strained SiGe islands on Si(001)

This article has been downloaded from IOPscience. Please scroll down to see the full text article.

2008 J. Phys.: Condens. Matter 20 454214

(http://iopscience.iop.org/0953-8984/20/45/454214)

View the table of contents for this issue, or go to the journal homepage for more

Download details:
IP Address: 129.252.86.83
The article was downloaded on 29/05/2010 at 16:12

Please note that terms and conditions apply.

J. Phys.: Condens. Matter **20** (2008) 454214 (7pp) doi:10.1088/0953-8984/20/45/454214

Intermixing and composition profiles of strained SiGe islands on Si(001)

A Rastelli[1], M Stoffel[1,2], T Merdzhanova[2] and O G Schmidt[1]

[1] Institute for Integrative Nanosciences, IFW Dresden, Helmholtzstraße 20, D-01069 Dresden, Germany
[2] Max-Planck-Institut für Festkörperforschung, Heisenbergstraße 1, D-70569 Stuttgart, Germany

E-mail: a.rastelli@ifw-dresden.de

Received 16 May 2008, in final form 4 July 2008
Published 23 October 2008
Online at stacks.iop.org/JPhysCM/20/454214

Abstract
We report on the experimental determination of composition profiles of strained three-dimensional (3D) SiGe islands on Si(001) substrates by means of a combination of selective wet chemical etching and atomic force microscopy (AFM). Isocompositional profiles at 65% Ge content were obtained by etching samples in a H_2O_2 solution. Quantitative 3D composition profiles of individual islands were extracted by using selective etching in a NH_4OH:H_2O_2 solution and an AFM-based nanotomography approach. This technique allows us to obtain at the same time 3D profiles for coherent and dislocated islands and to collect data with large statistics. Lateral and vertical composition gradients are observed and their origin is discussed.

(Some figures in this article are in colour only in the electronic version)

1. Introduction

Strain-driven self-assembly has attracted much attention during recent years since it provides a straightforward route to fabricate coherent, defect-free semiconductor 'quantum dots' (QDs). The SiGe/Si(001) system is considered as a prototypical example to study the formation mechanism [1, 2], the morphological evolution [3, 4], as well as the controlled nucleation of QDs [5–8]. During epitaxial growth, the deposited material intermixes with the substrate material [9–16], leading to a reduction of the lattice mismatch between the epilayer and the substrate and to the formation of alloyed islands. A precise knowledge of the material distribution in the islands is of particular importance for the prediction of the electronic and optical properties of novel devices based on SiGe islands [17]. The compositional state has thus been the subject of numerous experimental and theoretical investigations [18–21]. A powerful method to obtain 3D composition profiles for ensembles of islands is represented by anomalous x-ray scattering [14, 22, 23]. Cross-sectional transmission electron microscopy (TEM) combined with electron energy loss spectroscopy (EELS) [24, 25] has been used to address single islands but it is limited to cross-sectional profiles. Also x-ray photoemission electron microscopy (XPEEM) [13] allows single islands to be studied but its sensitivity is limited to the sample surface.

Selective wet chemical etching combined with atomic force microscopy (AFM) has emerged as a simple technique to probe the compositional state of islands [26–29, 15, 30], even after Si overgrowth [31].

In this paper, we first show that the etching rates of commonly used SiGe etchants are not significantly affected by strain. Isocomposition profiles of islands grown at relatively low substrate temperatures are revealed by selective wet chemical etching in a H_2O_2 solution and their origin discussed. Finally, we show that quantitative 3D composition profiles of individual islands can be obtained by combining AFM imaging of the same surface area after several etching steps in a NH_4OH:H_2O_2 solution and dedicated reconstruction algorithms.

2. Experiment

The samples investigated here were grown by solid source molecular beam epitaxy (MBE) on Si(001) substrates. After *ex situ* standard chemical cleaning and *in situ* deoxidation at 950 °C, the substrate temperature was ramped down to 460 °C and a 100 nm thick Si buffer was grown at a rate of 0.1 nm s^{-1} prior to Ge deposition at 580–740 °C. Within our growth conditions, the islands are alloyed and have different

 © 2008 IOP Publishing Ltd Printed in the UK

shapes. After growth, the samples were immediately cooled to room temperature for etching and imaging with a commercial AFM operated in the tapping mode. Selective wet chemical etching was performed at room temperature using either a 31% H_2O_2 solution, which is known to etch selectively $Si_{1-x}Ge_x$ alloys with $x > (65 \pm 5)\%$ [32], or a 1:1 vol (28% NH_4OH):(31% H_2O_2) solution (NHH), which etches selectively $Si_{1-x}Ge_x$ alloys at a rate increasing approximately exponentially with x [15]. The former solution was used to image isocompositional profiles of Ge-rich islands grown at low substrate temperature. The NHH solution was chosen to investigate the composition of islands with x less than ~40% because of its slow etching rate in this composition range, allowing us to perform controllable etching experiments. A possible mechanism responsible for the selective behavior of the NHH solution is discussed in [15]. Prior to each etching step, samples were dipped in a HF:H_2O (1:10) solution to remove the surface oxide. By comparing AFM images of the same surface area taken before and after deoxidization, we found that the HF dip does not produce any appreciable change in surface morphology, indicating a uniform removal of the surface oxide.

3. Etching rate calibration

Since SiGe islands are strained, it is important to check whether the etching rates are significantly affected by strain. To this end, we performed etching experiments on planar $Si_{1-x}Ge_x$ films having different compositions and strain states. The detailed sample structures are given in [33]. Rectangular structures were then fabricated using optical lithography followed by deposition of 20 nm of Cr. The latter were then used as an etch mask for the following etching steps. After each etching step, the same surface area was imaged and the resulting images were superimposed in order to have the same average height for the Cr surface at all etching times. We then determined the etched depth as follows: we define a sequence of images $\Delta\Gamma(t) = \Gamma(0) - \Gamma(t)$, where $\Gamma(0)$ represents the surface topography prior to etching. The average etched depth d is then taken as the mean value of $\Delta\Gamma(t)$ out of the Cr mesa. Figures 1(a) and (b) show the values of d obtained by this method for $Si_{1-x}Ge_x$ films etched in a NHH solution and having different compositions ($x = 0.4$, 0.6) and strain states (the meaning of the symbols is the same for all graphs) as a function of etching time t. It is obvious that, for a given composition, most of the data points lie on a straight line. For the sample with $x = 0.8$, a similar analysis was then performed using a H_2O_2 solution. The results are displayed in figure 1(c). Also in this case the data points lie on a straight line for both tensile strained and relaxed samples. However, a small deviation is observed for the compressively strained film. For this sample the etching rate of the NHH solution also appears higher than for the other samples with $x = 0.8$. Because of possible deviation of x from the nominal values and the strong dependence of the etching rates on x we may ascribe this difference to a slightly larger value of x. The etching rates r, which are then deduced by a linear fit with $d = rt$, are summarized in figure 1(d). For a given composition and for

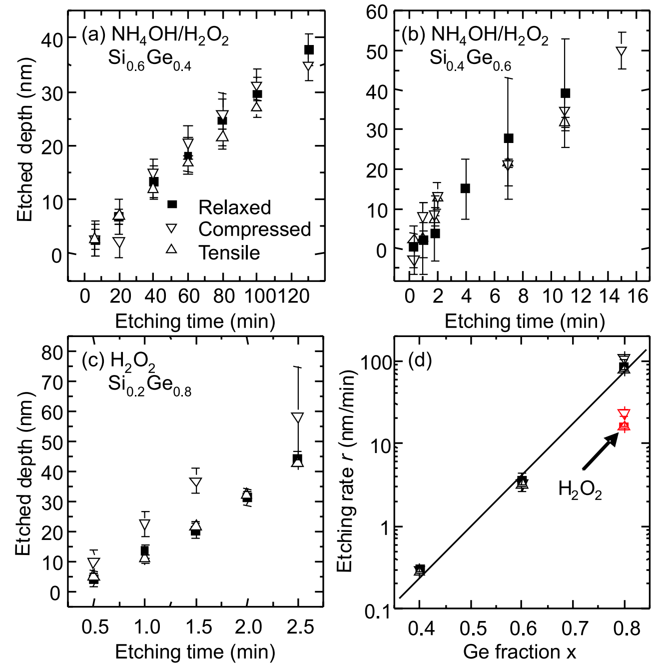

Figure 1. (a) and (b) Etched depth d as a function of etching time t determined by using a NHH solution for $Si_{1-x}Ge_x$ films with $x = 0.4$–0.6 and different strain states (the symbols used have the same meaning for all plots), (c) d as a function of t determined by using a H_2O_2 solution for $Si_{0.2}Ge_{0.8}$ films, (d) etching rate versus nominal film composition determined from the linear fits of the data points shown in (a)–(c).

both etchants considered in our study, we find that the etching rates are not significantly affected by strain since a biaxial strain as large as 0.84% does not produce significant changes in the etching rates [33]. In the following, we will show that selective wet chemical etching combined with AFM allows us to get a detailed insight into the lateral and vertical composition profiles of self-assembled islands.

4. Isocompositional profiles at 65% Ge

Figure 2(a) shows an AFM scan of a sample obtained upon deposition of 5.9 ML Ge at 580 °C. One can recognize a multimodal island distribution consisting of elongated, rectangular hut clusters (H) with edges aligned along ⟨100⟩ directions, square-based pyramids (P) bounded by four {105} facets and multifaceted dome islands (D).

Figure 2(b) shows the surface topography (of a different sample area) after 2 min etching in a H_2O_2 solution, while the lower part of figure 2 shows a 3D magnification of a single dome (figure 2(c)) and pyramid (figure 2(d)) after etching. Etched domes exhibit rather isotropic ring-like structures (figure 2(c)) or anisotropic profiles with only one etched side, such as those pointed at by arrows in figure 2(b). The observation of ring-like structures suggests that the dome periphery is Si-rich while the center and the apex are more Ge-rich. In post-growth annealed samples, most of the etched domes have an anisotropic shape, which results from a surface-mediated alloying accompanied by lateral island motion on the

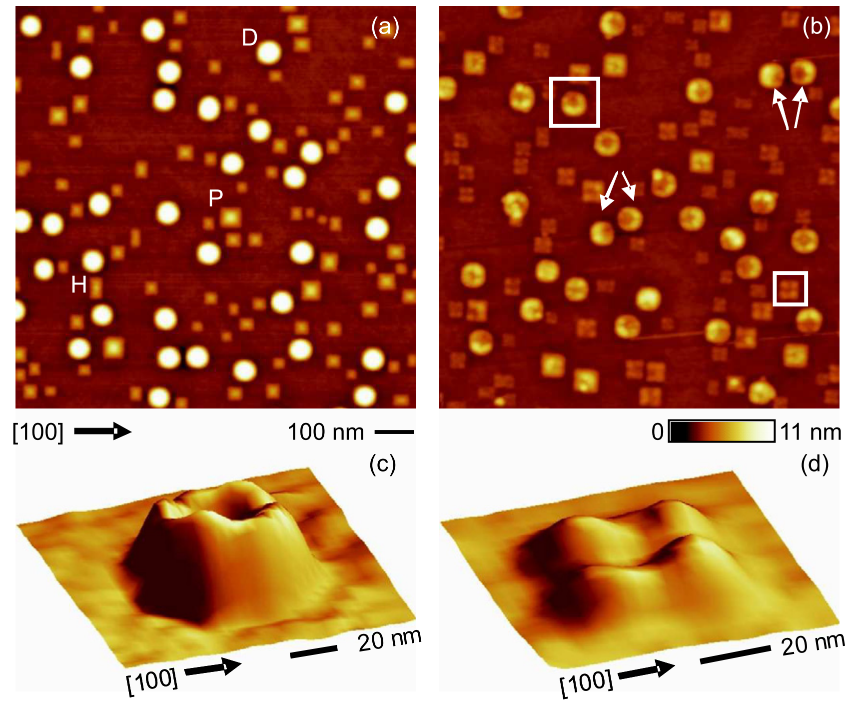

Figure 2. (Color online) AFM scans of a sample obtained upon deposition of 5.9 ML Ge at 580 °C prior to (a) and after etching for 2 min in a 31% H_2O_2 solution (b). 3D magnifications of the etched dome (c) and the pyramid (d) marked by squares in (b).

substrate surface during annealing [29]. In the case discussed here, where the sample was immediately cooled to room temperature after deposition, we mainly observe isotropic ring-like structures. However, anisotropic shapes are observed when neighboring islands are sufficiently close to each other. We expect that the repulsive strain fields between neighboring islands trigger the lateral motion [34], giving rise to the observed anisotropic composition profiles.

A careful inspection of the etched pyramids (figure 2(d)) reveals that their height is reduced and that four mounds remain at the corners of the former pyramids. In addition, a depression is observed in the middle of the pyramids. Our observations thus imply that the pyramid corners are Si-rich while the Ge-rich regions correspond to the center, the apex and the edges of the pyramids. The observed composition profile cannot be interpreted by an elastic strain energy minimization [26]. Instead, a simple kinetic model based on surface interdiffusion during growth [26, 28] is able to reproduce correctly the experimentally observed lateral composition profiles for both domes and pyramids, thus underlining the importance of surface diffusion processes. Interestingly, the lateral composition profile is qualitatively the same both for freshly grown and annealed SiGe pyramids [26] suggesting that the pyramids do not move laterally on the substrate surface. A possible explanation is that when both shallow and steep islands are present on the surface, strain relaxation in the film can take place by coarsening (with large and steep islands growing at the expense of small and shallow islands). Intermixing through lateral motion mainly takes place for islands with steep morphology, which cannot grow further without dislocation introduction. A detailed discussion on this scenario can be found in [35].

Based on the results discussed above we can conclude that selective etching combined with AFM is able to provide information on the composition profiles of individual islands. Such results were found to be compatible with those obtained by anomalous x-ray scattering on large island ensembles [23]. It seems, however, that the H_2O_2 solution can at most provide isocompositional profiles and not the full 3D composition profiles of islands. The monotonic dependence of the etching rate of the NHH solution on the Ge fraction x (see figure 1(d)) suggests a possible way to reconstruct the composition from the measurement of the etching rate, as discussed in section 5.

5. 3D composition profiles

In order to determine the local etching rate for different regions of the same sample we used a 'nanotomography' approach, similar to that employed by Magerle [36] to reveal the 3D shape of buried nanostructures. The method consists of etching a sample several times and measuring, by AFM, the evolution of the topography of the same sample area.

Figure 3(a) shows a 3D view of an AFM topograph of a sample obtained by depositing 15 ML Ge at a substrate temperature of 740 °C. Most of the islands are coherent domes and islands with an intermediate shape between domes and steeper barns (TBs) [4]. Plastically-relaxed superdomes (SDs) are also observed because of the large amount of deposited Ge. A few transition islands (TDs) with intermediate morphology between shallow Ps and Ds are also observed. Different island shapes are pointed at by arrows.

Islands are surrounded by trenches which penetrate into the Si substrate [10, 37] and are clearly visible at any etching step. Besides providing valuable information on the island

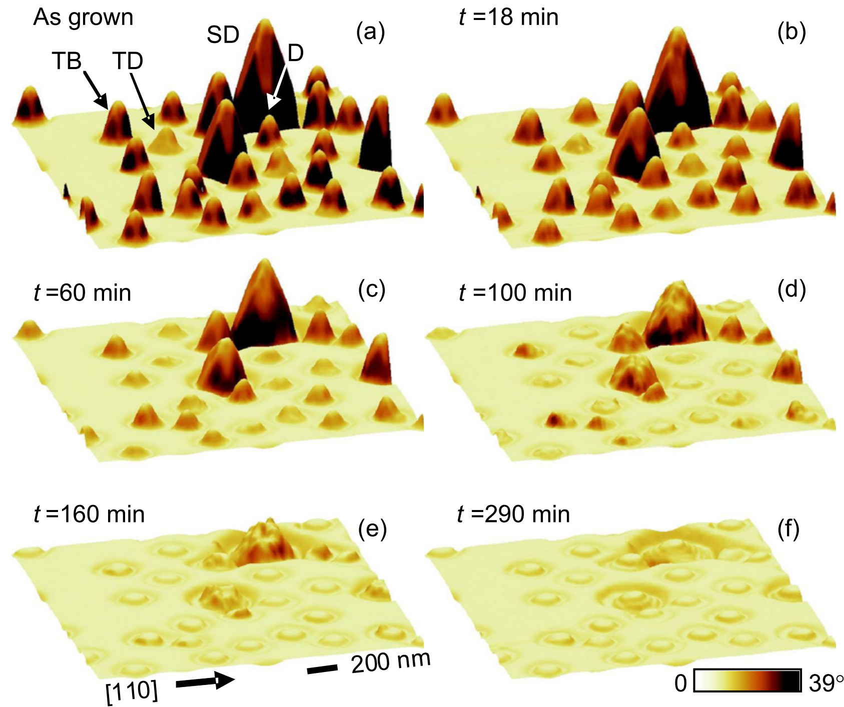

Figure 3. (Color online) (a)–(f) Sequence of AFM images (3D views) of the same surface area of a sample obtained by depositing 15 ML Ge on Si(001) at 740 °C and selectively etched in a NHH solution for the indicated time t.

evolution during growth [38] and allowing us to discriminate between coherent and dislocated islands [39], such trenches were used here as 'markers' to align the images taken at etching time t_i with the image taken before etching. (Interpolation was applied to compensate for the non-linearities of the open-loop AFM scanner used here[3].) Figures 3(b)–(f) show some of the resulting images taken at increasing t. While the surface is smooth prior to etching (figure 3(a)) and after complete removal of the SiGe material (figure 3(f)), the surface of partially etched islands shows some random 'bumps', which we attribute to etching-induced roughening. While roughening of the etched front will affect the ultimate spatial resolution achievable with the method, it is not relevant for the conclusions drawn here.

In order to reconstruct the local etching rate in 3D, for each point P belonging to the surface $\Gamma(t_i)$ measured at t_i we assumed that P evolves into the nearest point Q on the surface $\Gamma(t_{i+1})$ during etching. We therefore assigned to the segment PQ a local etching rate $r_{PQ} = \overline{PQ}/(t_{i+1} - t_i)$.

From the local etching rate values obtained in this way we can estimate the local composition by using the rate calibration data shown in figure 1(d). To obtain an analytic relation between r and x we fitted the data with a phenomenological function $x = a + b\log(r)$. The result of the fit, with the corresponding error, were then used to calculate the composition (with its uncertainty) of each point of the islands.

[3] The image correction, alignment, tomography computation and visualization were obtained by a software package based on the ITT-IDL Platform. The source can be downloaded at http://www.ifw-dresden.de/institutes/iin/members/ar5.

To display the local composition, we constructed a 3D matrix, with each voxel (bin or pixel in 3D) Ω_{ijk} being assigned a value $x_{ijk} = a + b\log(r_{ijk})$, where r_{ijk} is the mean etching rate of the points belonging to Ω_{ijk}. The choice of the voxel size is rather arbitrary and different choices were found to produce similar results. By taking into account the finite size of the AFM probe, the pixels in the AFM images and the roughness developing during etching, we fixed the lateral and vertical resolution to 19 nm (twice the size of the pixels of the original AFM image) and 4 nm (slightly more than the typical amount of material removed after each etching step), respectively.

Figure 4 shows some of the results of this analysis for the islands marked in figure 3(a). Figures 4(a)–(d) show cross-sections through the centers of different island types, shown in the corresponding insets. The values of the local composition x_{ijk} are color-coded. Both for coherent and dislocated islands, the Ge fraction drops moving from the island top towards the substrate, as quantified on the right panels of figure 4 where the average Ge fraction at constant height z is plotted as a function of the distance from the substrate level (at $z = 0$). This is consistent with data previously obtained by other methods on the SiGe system [23, 27, 25] and also on other material systems [40]. Furthermore, for the coherent islands present on the sample, we found quantitative agreement between the values of x obtained by nanotomography and those obtained by anomalous x-ray scattering [30].

A detailed analysis performed on more than 100 islands show that the Ge fraction through the island axes (i.e. through a vertical line passing through the center of the island base) have absolute values which depend on z, but not on the particular

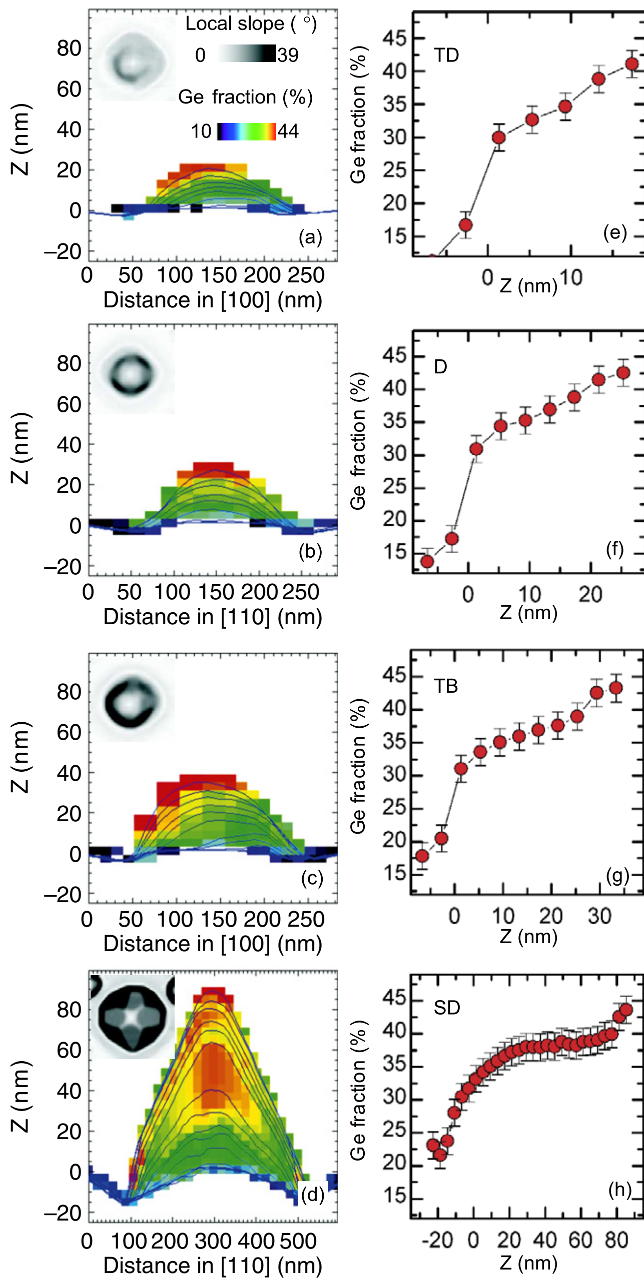

Figure 4. (Color online) (a)–(d) Cross-cuts through the centers of the islands shown in the corresponding insets and taken either along the [110] (parallel to the insets edges) or to the [100] directions. The values of composition are color-coded. Linescans through the original AFM images used to compute the local Ge fraction are also shown as lines. (e)–(h) Average x as a function of z for the islands shown in (a)–(d). $z = 0$ corresponds to the substrate level.

island size and shape. In particular, the regions of the islands with small z, uncovered at different etching times depending on the initial island size, have similar x [30]. This observation can be understood by considering that under our experimental conditions intermixing takes place mainly through surface diffusion [26, 19, 16]. Therefore the composition of the material buried inside an island does not change appreciably during the evolution of its surface. If we keep in mind that large islands are the result of the growth of small islands by accumulation of material at their surface [41], we can conclude that the initial pyramids are Si-rich, possibly because of the substantial contribution of the alloyed WL to their growth [42, 43].

Besides vertical gradients in composition, figures 4(a)–(d) also show lateral variations. For coherent islands such as TDs and TBs (figures 4(a) and (c)) we find that the lateral composition profile is generally asymmetric and we attribute this observation to surface-mediated alloying accompanied by a slight lateral motion [26]. Since the sample was not intentionally annealed after growth, the lateral motion can hardly be detected from the analysis of the trenches left by the islands on the substrate [38]. For domes, the shape and composition tend to be more symmetric (figure 4(b)). For superdomes, we observe a Ge-rich core surrounded by a Si-rich shell close to the island base (figure 4(d)). Such a shell is probably due to Si which is expelled from the deep trench at the island base and 'climbs' the superdome walls (see below).

With the nanotomography approach we can state that AFM becomes an analytic tool and we can combine the typical results obtained from the analysis of AFM topographs, such as island size and shape with the—so far unknown—island average composition $\overline{x}$. The latter is simply estimated by averaging x over all the matrix voxels belonging to a given island and is plotted in figure 5(a) as a function of island volume. It is evident that small (and shallow) islands are generally Si-richer than large (and possibly dislocated) islands. Such a trend can be rationalized by the fact that both steep and dislocated islands are less strained than shallow islands and thus represent more favorable locations for the accumulation of Ge. On the other hand, larger islands exert an increasing stress on the Si substrate, promoting the formation of wider and deeper trenches at their feet. The Si expelled from the trenches can be incorporated in the growing islands, thus partially compensating the Ge enrichment [26].

Since the last image taken during the etching sequence (at $t_f = 290$ min) represents to a good approximation the profile of the Si substrate, we subtracted the substrate level from the image collected prior to etching and thus obtained the volume V_{SiGe} of only the SiGe material composing the islands. By evaluating the volume of Si removed from the trench below and surrounding each island V_{Trench}, we can quantify the impact of this Si source on the island composition. By plotting the ratio $V^*_{\mathrm{Trench}} = V_{\mathrm{Trench}}/[(1-\overline{x})V_{\mathrm{SiGe}}]$ as a function of island volume V_{SiGe} (figure 5(b)), we see that trenches provide about 40% of the Si contained in coherent (TDs, Ds, TBs) and small dislocated islands with up to 2–3 dislocations (SSDs) and up to about 65% of the Si contained in the large superdomes (SDs). The remaining Si must therefore originate from other areas of the substrate through long-range diffusion [37, 29, 15].

6. Conclusions

In this work we have discussed the application of selective wet chemical etching combined with scanning probe microscopy as a tool to obtain information on the composition profiles of strained SiGe/Si(001) islands. Since strain could possibly affect the etching rates, we have first shown that this

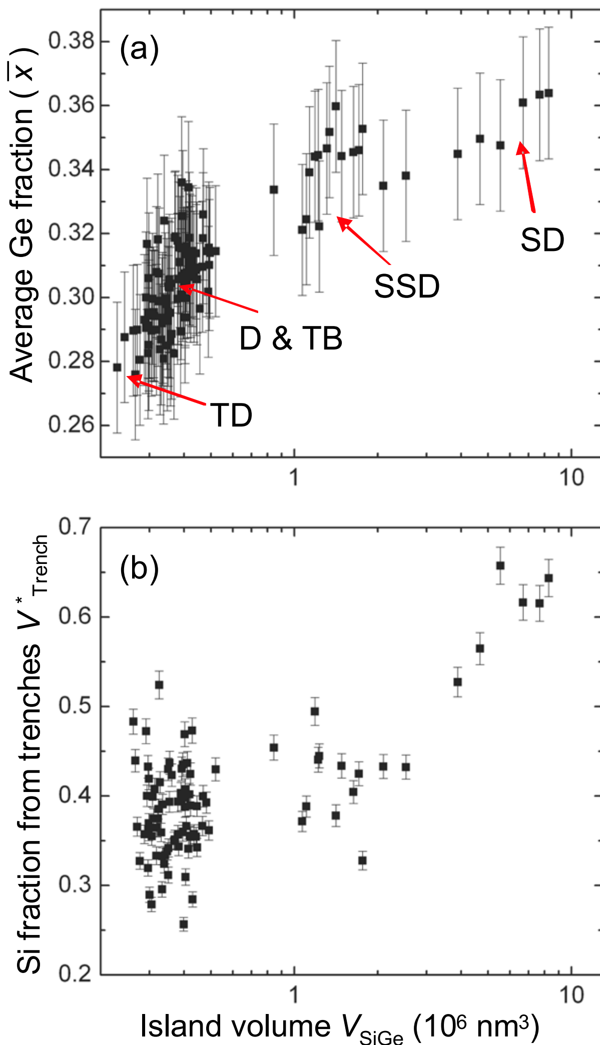

Figure 5. (a) Average Ge fraction $\bar{x}$ for more than 100 islands as a function of island volume V_{SiGe}. (b) Si fraction originating from the trenches V^*_{trench} as a function of V_{SiGe}.

is not the case using two etching solutions which are commonly employed to study the composition of SiGe layers. Isocomposition profiles for both pyramids and domes revealed by etching in a H_2O_2 solution were presented and discussed. By using a nanotomography approach based on an NHH solution, we have demonstrated that we can get access to the full 3D composition profiles of strained SiGe/Si(001) islands. We expect that this approach can yield valuable information for the design of devices based on single SiGe islands. Based on the availability of suitable etchants the approach can be possibly extended to other strained material combinations.

Acknowledgments

The authors thank G Katsaros, A Malachias, U Denker, M S Leite, G Medeiros-Ribeiro, L Miglio, F Montalenti, G Bauer and J Tersoff for fruitful discussions. G Isella, D Chrastina and H von Känel are acknowledged for providing SiGe samples used for the etching rate calibration. This work was supported by the BMBF (No. 03X5518), the EU project D-DotFET (No. 012150) and the DFG (FOR 730).

References

[1] Vailionis A, Cho B, Glass G, Desjardins P, Cahill D G and Greene J E 2000 *Phys. Rev. Lett.* **85** 3672
[2] Tersoff J, Spencer B J, Rastelli A and von Känel H 2002 *Phys. Rev. Lett.* **89** 196104
[3] Medeiros-Ribeiro G, Bratkovski A M, Kamins T I, Ohlberg D A A and Williams R S 1998 *Science* **279** 353
[4] Stoffel M, Rastelli A, Tersoff J, Merdzhanova T and Schmidt O G 2006 *Phys. Rev.* B **74** 155326
[5] Borgström M, Zela V and Seifert W 2003 *Nanotechnology* **14** 264
[6] Zhong Z, Halilovic A, Fromherz T, Schäffler F and Bauer G 2003 *Appl. Phys. Lett.* **82** 4779
[7] Kar G S, Kiravittaya S, Stoffel M and Schmidt O G 2004 *Phys. Rev. Lett.* **93** 246103
[8] Zhang J J, Stoffel M, Rastelli A, Schmidt O G, Jovanović V, Nanver L K and Bauer G 2007 *Appl. Phys. Lett.* **91** 173115
[9] Chaparro S A, Drucker J, Zhang Y, Chandrasekhar D, McCartney M R and Smith D J 1999 *Phys. Rev. Lett.* **83** 1199
[10] Kamins T I, Medeiros-Ribeiro G, Ohlberg D A A and Stanley Williams R 1999 *J. Appl. Phys.* **85** 1159
[11] Liao X Z, Zou J, Cockayne D J, Qin J, Jiang Z M, Wang X and Leon R 1999 *Phys. Rev.* B **60** 15605
[12] Capellini G, de Seta M and Evangelisti F 2001 *Appl. Phys. Lett.* **78** 303
[13] Ratto F, Rosei F, Locatelli A, Cherifi S, Fontana S, Heun S, Szkutnik P-D, Sgarlata A, de Crescenzi M and Motta N 2005 *J. Appl. Phys.* **97** 3516
[14] Schülli T U, Stoffel M, Hesse A, Stangl J, Lechner R T, Wintersberger E, Sztucki M, Metzger T H, Schmidt O G and Bauer G 2005 *Phys. Rev.* B **71** 035326
[15] Katsaros G, Rastelli A, Stoffel M, Isella G, von Känel H, Bittner A M, Tersoff J, Denker U, Schmidt O G, Costantini G and Kern K 2006 *Surf. Sci.* **600** 2608
[16] Leite M S, Medeiros-Ribeiro G, Kamins T I and Williams R S 2007 *Phys. Rev. Lett.* **98** 165901
[17] Schmidt O G and Eberl K 2001 *IEEE Trans. Electron Devices* **48** 1175
[18] Hadjisavvas G and Kelires P C 2005 *Phys. Rev.* B **72** 075334
[19] Tu Y and Tersoff J 2007 *Phys. Rev. Lett.* **98** 096103
[20] Medeiros-Ribeiro G and Williams R S 2007 *Nano Lett.* **7** 223
[21] Medhekar N V, Hegadekatte V and Shenoy V B 2008 *Phys. Rev. Lett.* **100** 106104
[22] Magalhães-Paniago R, Medeiros-Ribeiro G, Malachias A, Kycia S, Kamins T I and Williams R S 2002 *Phys. Rev.* B **66** 245312
[23] Malachias A, Kycia S, Medeiros-Ribeiro G, Magalhães-Paniago R, Kamins T I and Williams R S 2003 *Phys. Rev. Lett.* **91** 176101
[24] Müller E, Kirfel O, Rastelli A, von Känel H and Grützmacher D 2001 *Microscopy of Semiconducting Materials* ed A G Cullis and J L Hutchison (Bristol: Institute of Physics Publishing) p 163
[25] Floyd M, Zhang Y, Driver K P, Drucker J, Crozier P A and Smith D J 2003 *Appl. Phys. Lett.* **82** 1473
[26] Denker U, Stoffel M and Schmidt O G 2003 *Phys. Rev. Lett.* **90** 196102
[27] Schülli T U, Stangl J, Zhong Z, Lechner R T, Sztucki M, Metzger T H and Bauer G 2003 *Phys. Rev. Lett.* **90** 066105
[28] Katsaros G, Costantini G, Stoffel M, Esteban R, Bittner A M, Rastelli A, Denker U, Schmidt O G and Kern K 2005 *Phys. Rev.* B **72** 195320

[29] Denker U, Rastelli A, Stoffel M, Tersoff J, Katsaros G, Costantini G, Kern K, Jin-Phillipp N Y, Jesson D E and Schmidt O G 2005 *Phys. Rev. Lett.* **94** 216103
[30] Rastelli A, Stoffel M, Malachias A, Merdzhanova T, Katsaros G, Kern K, Metzger T H and Schmidt O G 2008 *Nano Lett.* **8** 1404
[31] Katsaros G, Stoffel M, Rastelli A, Schmidt O G, Kern K and Tersoff J 2007 *Appl. Phys. Lett.* **91** 013112
[32] Schmidt O G, Denker U, Christiansen S and Ernst F 2002 *Appl. Phys. Lett.* **81** 2614
[33] Stoffel M, Malachias A, Merdzhanova T, Cavallo F, Isella G, Chrastina D, von Känel H, Rastelli A and Schmidt O G 2008 *Semicond. Sci. Technol.* **23** 085021
[34] Stoffel M, Rastelli A, Kiravittaya S and Schmidt O G 2005 *Phys. Rev.* B **72** 205411
[35] Stoffel M, Rastelli A, Stangl J, Merdzhanova T, Bauer G and Schmidt O G 2007 *Phys. Rev.* B **75** 113307
[36] Magerle R 2000 *Phys. Rev. Lett.* **85** 2749
[37] Denker U, Schmidt O G, Jin-Philipp N-Y and Eberl K 2001 *Appl. Phys. Lett.* **78** 3723
[38] Rastelli A, Stoffel M, Katsaros G, Tersoff J, Denker U, Merdzhanova T, Kar G S, Costantini G, Kern K, von Känel H and Schmidt O G 2006 *Microelectron. J.* **37** 1471
[39] Merdzhanova T, Kiravittaya S, Rastelli A, Stoffel M, Denker U and Schmidt O G 2006 *Phys. Rev. Lett.* **96** 226103
[40] Kegel I, Metzger T H, Lorke A, Peisl J, Stangl J, Bauer G, Nordlund K, Schoenfeld W V and Petroff P M 2001 *Phys. Rev.* B **63** 035318
[41] Montalenti F, Raiteri P, Migas D B, von Känel H, Rastelli A, Manzano C, Costantini G, Denker U, Schmidt O G, Kern K and Miglio L 2004 *Phys. Rev. Lett.* **93** 216102
[42] Schmidt O G, Lange C and Eberl K 1999 *Appl. Phys. Lett.* **75** 1905–7
[43] Schülli T U, Richard M-I, Renaud G, Favre-Nicolin V, Wintersberger E and Bauer G 2006 *Appl. Phys. Lett.* **89** 162105